Supplemental Information

miR-142 Controls Metabolic Reprogramming that Regulates Dendritic Cell Activation

Yaping Sun, Katherine Oravecz-Wilson, Sydney Bridges, Richard McEachin, Julia Wu, Stephanie H. Kim, Austin Taylor, Cynthia Zajac, Hideaki Fujiwara, Israel Henig, Daniel Christopher Peltier, Thomas Saunders, and Pavan Reddy

Supplemental Data Items

Figure S1: *miR-142*$^{-/-}$ mice displayed an impairment of both CD4^{+} and CD8^{+} DC homeostasis

DCs were purified from splenocyes isolated from WT or *miR-142*$^{-/-}$ mice using CD11c Microbeads and treated with or without LPS (500 ng/ml) for indicated time. DCs were harvested for FACS staining using antibodies against CD4 and CD8. Data obtained from 3 independent experiments were presented as mean ± SEM by mean fluorescence intensity (MFI).

Figure S2: Analysis of gene set for glycolysis pathway

(A). Affymetrix microarrays were processed and data were analyzed as described in Methods. Enrichment score of gene set for glycolysis pathway in WT and *miR-142*$^{-/-}$ DCs was analyzed by GSEA. Data were obtained from 3 biological triplicates in each group. Enrichment plot (top panel) and ranked gene list correlation profiles (bottom panel) were shown. (B) AMPK activation in WT and *miR-142*$^{-/-}$ DCs untreated or treated with LPS for indicated time was examined by Western blot. Densitometry Data (mean ± SEM) were pooled from 3 independent experiments. (C) After treated with LPS for 6 hrs, activation of AKT and PRAS (30 min) or STAT3 in WT and *miR-142*$^{-/-}$ DCs were examined by Western blot. Densitometry data were combined from 3 similar and independent experiments (mean ± SEM). Comparisons between 2 groups were calculated using paired Student *t* test (two-tailed), while comparisons between 2 groups at

multiple time points were calculated utilizing Multiple *t* tests (the Holm-Sidak method). *p<0.05; **p<0.01, NS: not significant.

Figure S3. GSEA analysis of gene set for oxidative phosphorylation (OXPHOS) pathway

Affymetrix microarrays were processed and data were analyzed as described in Methods. Enrichment score of gene set for oxidative phosphorylation (OXPHOS) pathway in WT and *miR-142*$^{-/-}$ DCs was analyzed by GSEA. Data were obtained from 3 biological triplicates in each group. Enrichment plot (top panel) and ranked gene list correlation profiles (bottom panel) were shown.

Figure S4. GSEA analysis of gene set for tricarboxylic acid cycle (TAC) pathway

(A) Affymetrix microarrays were processed and data were analyzed as described in Methods. Enrichment score of gene set for tricarboxylic acid cycle (TAC) pathway in WT and *miR-142*$^{-/-}$ DCs was analyzed by GSEA. Enrichment scores were obtained from 3 biological triplicates in each group. (B) Enrichment plot (top panel) and ranked gene list correlation profiles (bottom panel) are shown.

Figure S5. GSEA analysis of gene set for Fatty acid oxidation (FAO) pathway

Affymetrix microarrays were processed and data were analyzed as described in Methods. Enrichment score of gene set for Fatty acid oxidation (FAO) pathway in WT and *miR-142*$^{-/-}$ DCs was analyzed by GSEA. Enrichment plot (top panel) and ranked gene list correlation profiles (bottom panel) were shown.

Figure S6: Computational prediction of miR-142 Targets

Alignments of miR-142 and its computational predicted targets CPT1a, FABP4, FABP5, Ndufs7, and Uqcrb were shown.

Figure S7: FA uptake is increased in *miR-142*$^{-/-}$ DCs

(A-C) As the supplementary data for Figure 7A (6 hrs), WT and *miR-142*$^{-/-}$ DCs were untreated or treated with LPS for 1, 2, 4 or 6 hrs, FA uptake at 20 sec intervals for 30 min was determined by fluorescence reader as described in Methods. Data obtained for 1, 2 and 4 hrs treatment were combined from 3 independent experiments and presented as mean ± SEM. Comparisons between 2 groups at multiple time points were calculated utilizing Multiple *t* tests (the Holm-Sidak method). *p<0.05; **p<0.01, NS: not significant.

Figure S8: Fatty acid transporter proteins are increased in *miR-142*$^{-/-}$ DCs

(A) WT and *miR-142*$^{-/-}$ DCs were untreated or treated with LPS for indicated time. Whole cell lysates were processed for immunoblotting using antibodies against FABP4, FABP5 and β-Actin as in Figure 7B. Densitometry data combined from 3 independent experiments were presented as mean ± SEM. (B) WT and *miR-142*$^{-/-}$ DCs were untreated or treated with LPS for indicated time. Whole cell lysates were processed for immunoblotting using antibodies against FATP1, FATP4 and β-Actin. A presentative image of Western blot is shown (top). Densitometry data for FABP1 (middle) and FABP4 (bottom) combined from 3 independent experiments are presented as mean ± SEM (paired Student's t test). (C) WT and *miR-142*$^{-/-}$ DCs were untreated or treated with LPS for indicated time. Whole cell lysates were processed for immunoblotting using antibodies against Ndufs7, Uqcrb and β-Actin as in Figure 7D. Densitometry data combined from 3 independent experiments are presented as mean ± SEM. Comparisons between 2 groups at multiple time points were calculated utilizing Multiple *t* tests (the Holm-Sidak method). *p<0.05; **p<0.01, NS: not significant.

Figure S9: Restoration of miR-142 expression in *miR-142*$^{-/-}$ DCs

(A) Restoration of miR-142 expression in miR-142$^{-/-}$ DCs *miR-142*$^{-/-}$ DCs were transfected with lentiviral miR-142 or control vectors facilitated with viral transduction enhancer G698. For miRNA quantitative PCR, total RNA including small RNAs isolated using the miRNeasy Mini Kit (QIAGEN) from DCs. Specific RT primers for miR142-3p, miR-142-5p and snoRNA135 (control) were used and qPCR was performed as described in Methods. Data were combined from 2 independent experiments and presented as mean ± SEM. **(B)** Densitometry data as shown in Figure 6 E were combined from 3 independent experiments (mean ± SEM). Comparisons between 2 groups were calculated using paired Student *t* test (two-tailed). *p<0.05; **p<0.01, NS: not significant.

Figure S10 miR-142 deficiency induced changes in FA Metabolism are critical for modulation of DC functions

(A-D) WT and *miR-142*$^{-/-}$ DCs were untreated or treated with LPS, 2-DG or/and etomoxir for 24 hrs. Culture media were collected for measuring the cytokine concentration by ELISA as in Figure 7. The relative expression (%) calculated by subtracting the cytokine values after 2-DG or /and etomoxir treatment from the cytokine values obtained by LPS stimulation only. Data were obtained from 3 independent experiments and presented as mean ± SEM. **(E)** Model for miR142 regulation of DCs' metabolism which favors FAO and OXPHOS, and leads to tolerogenic state in *miR-142*$^{-/-}$ DCs. **(F)** After T cells, which were purified from either WT B6 mice or *miR-142*$^{-/-}$ mic, were treated with CD3/CD28 Dynabeads (10µl/10^6 cells) for 3 days, or macrophages, derived from bone marrow isolated from WT B6 mice or *miR-142*$^{-/-}$ mice, were treated with LPS (500ng/ml) for 24 hrs, CPT1a expression was examined by Western blot (left).

Densitometry data (right) were combined from 3 similar and independent experiments (mean ± SEM). Comparisons between 2 groups were calculated using paired Student t test (two-tailed). *p<0.05; **p<0.01, NS: not significant (paired Student's *t* μtest).

Figure S1: WT and *miR-142*$^{-/-}$ mice displayed similar subsets of CD4^{+} and CD8^{+} CD11c^{+} DC homeostasis

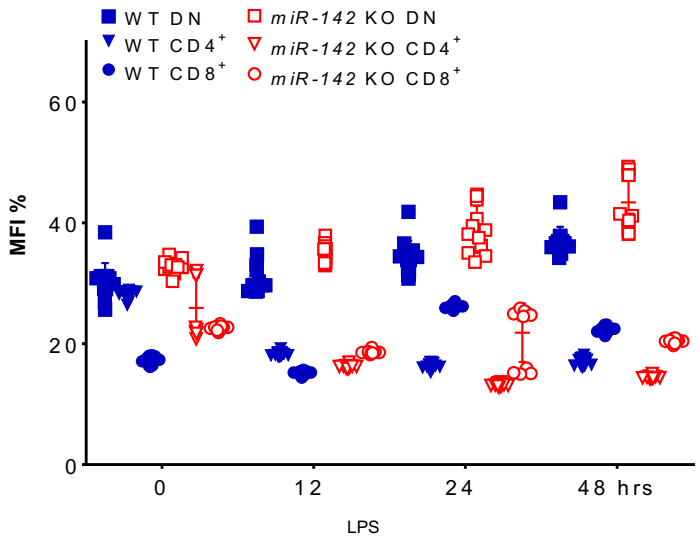

Figure S2: GSEA analysis of gene set for glycolysis pathway

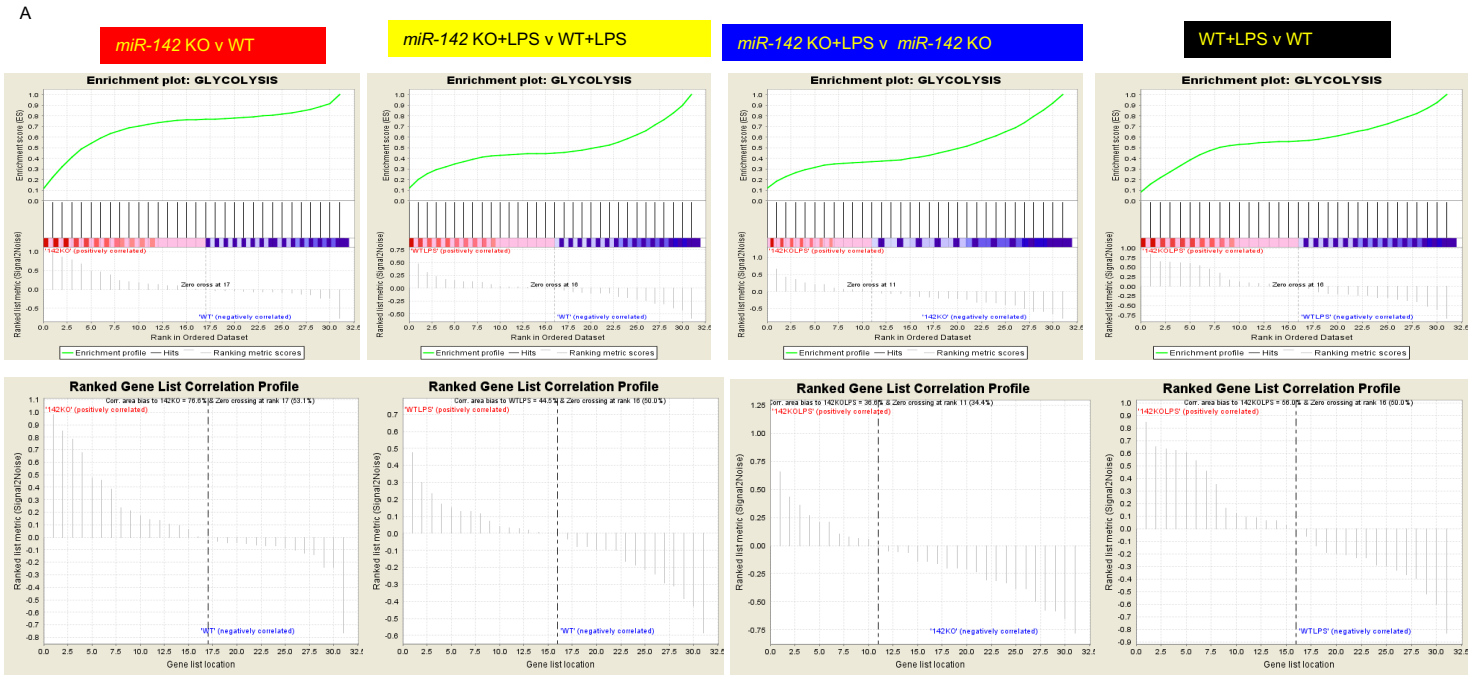

Figure S3: GSEA analysis of gene set for oxidative phosphorylation (OXPHOS) pathway

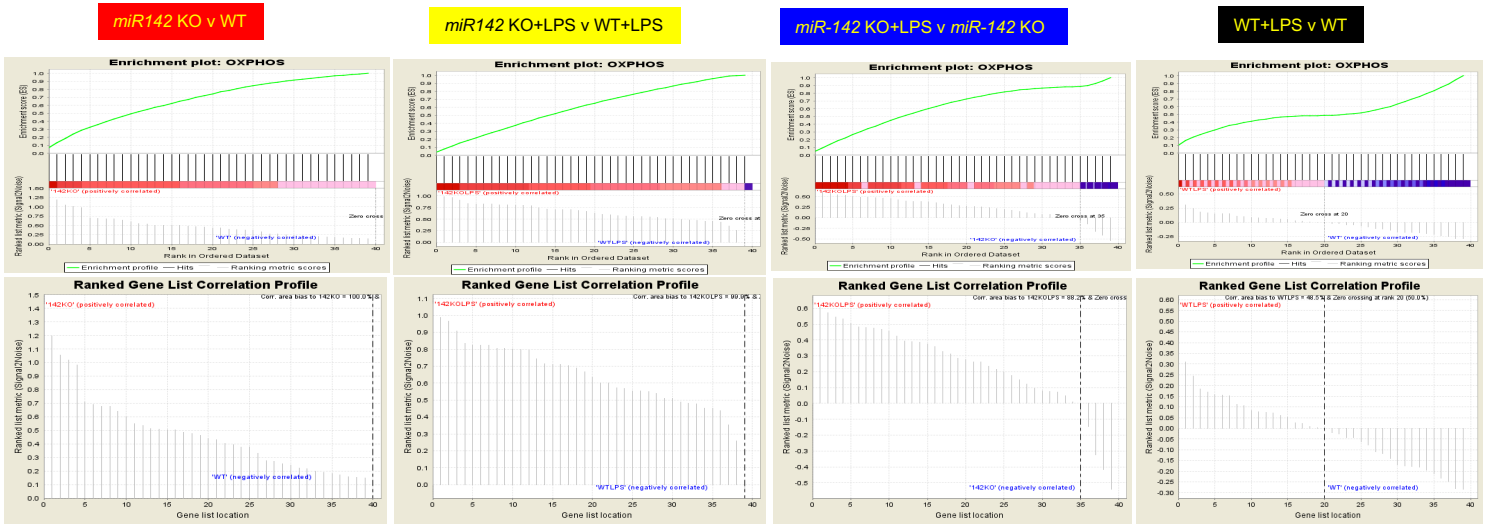

Figure S4: GSEA analysis of gene set for tricarboxylic acid cycle (TAC) pathway

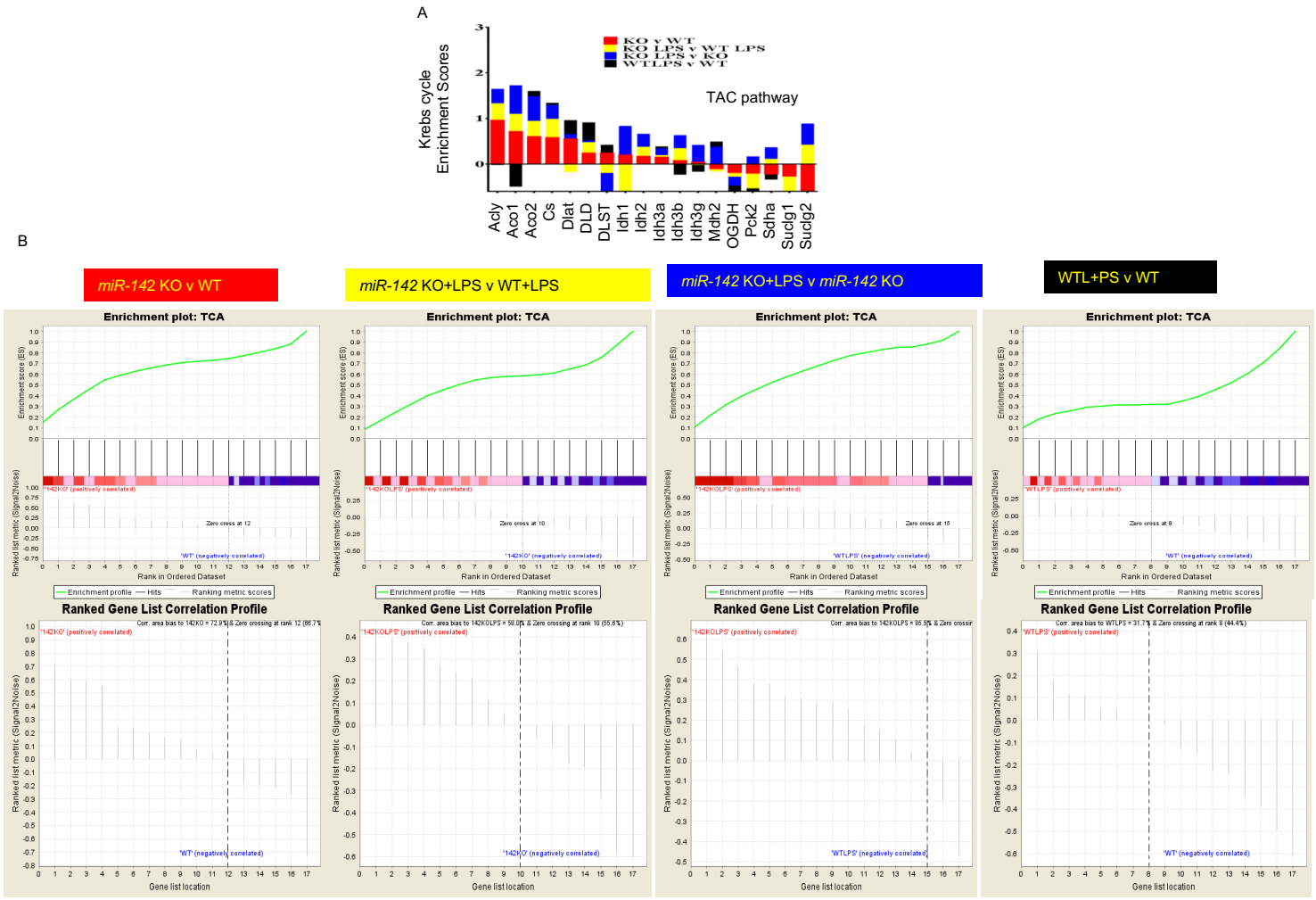

Figure S5: Fatty acid oxidation (FAO) pathway

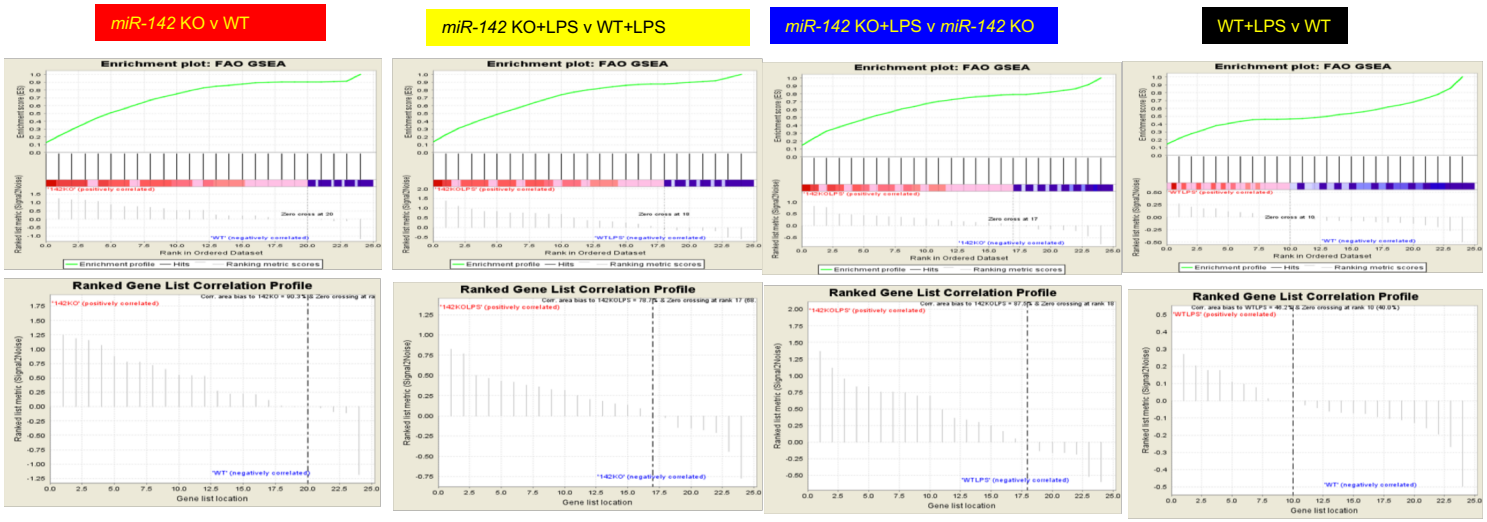

Figure S6: Computational prediction of miR-142 Targets

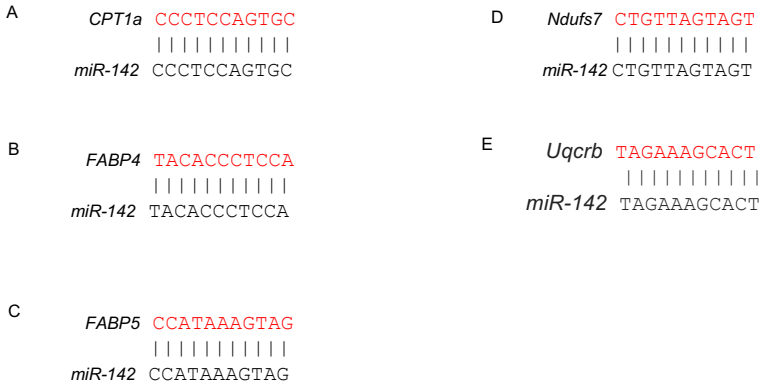

Figure S7: FA uptake is increased in *miR-142*$^{-/-}$ DCs

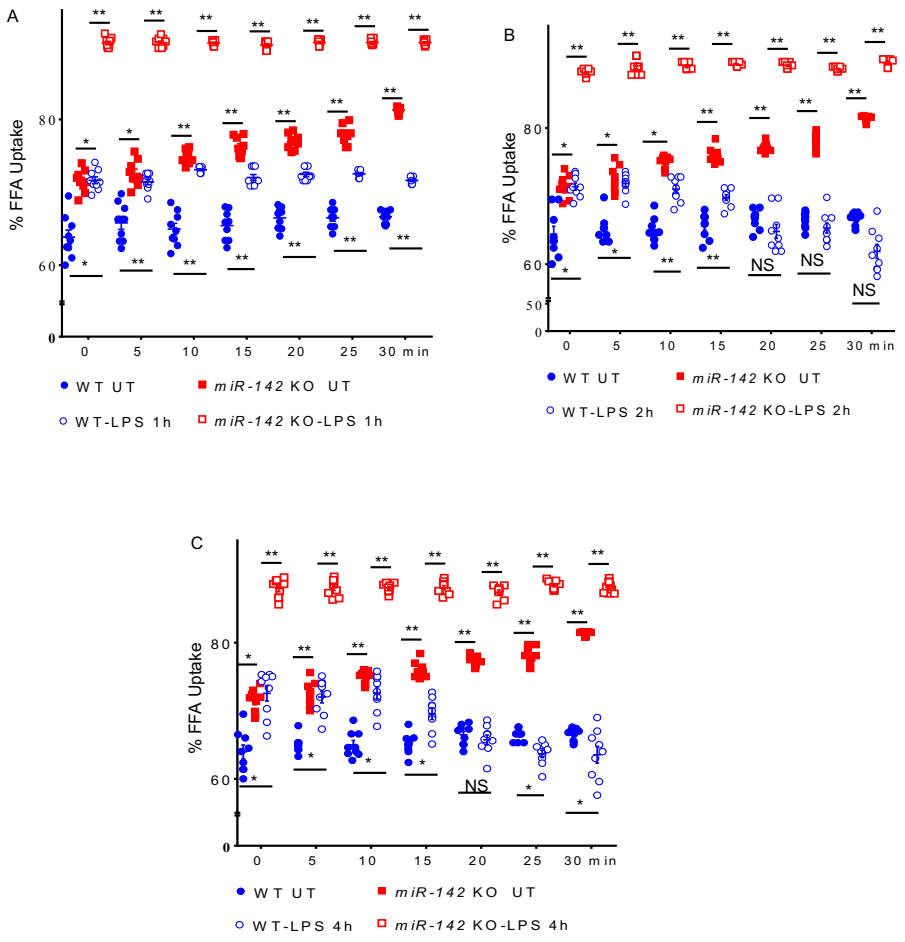

Figure S8: Fatty acid transporter proteins are increased in *miR-142*$^{-/-}$ DCs

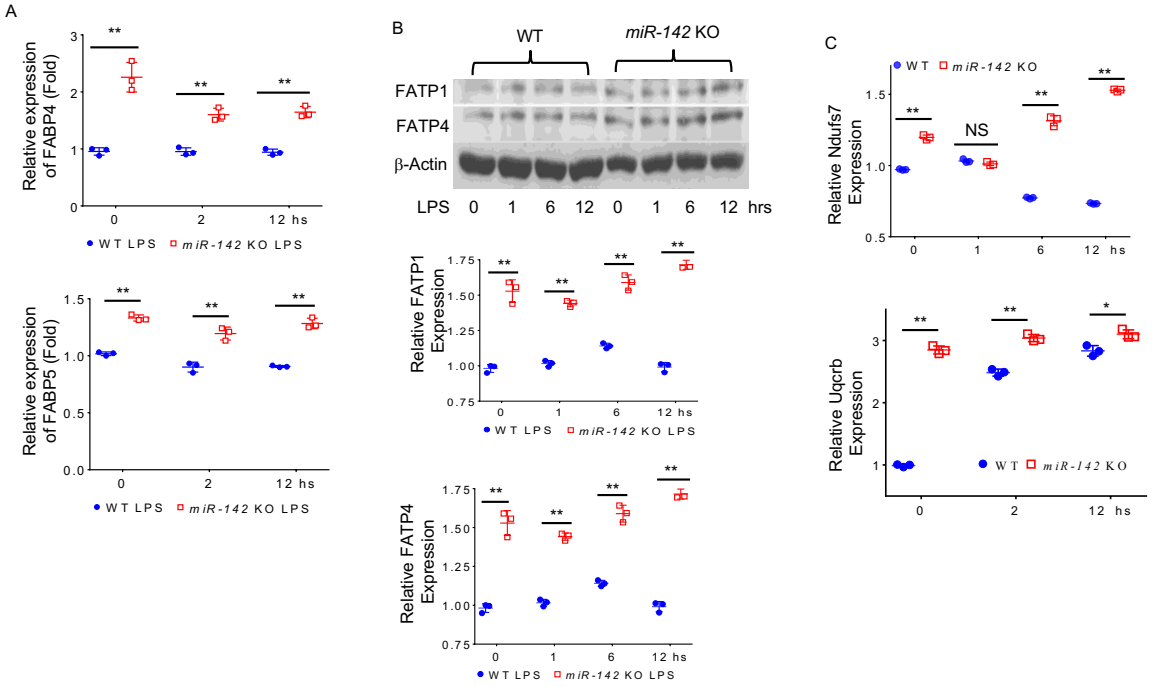

Figure S9: Restoration of miR-142 expression in *miR-142* KO DCs

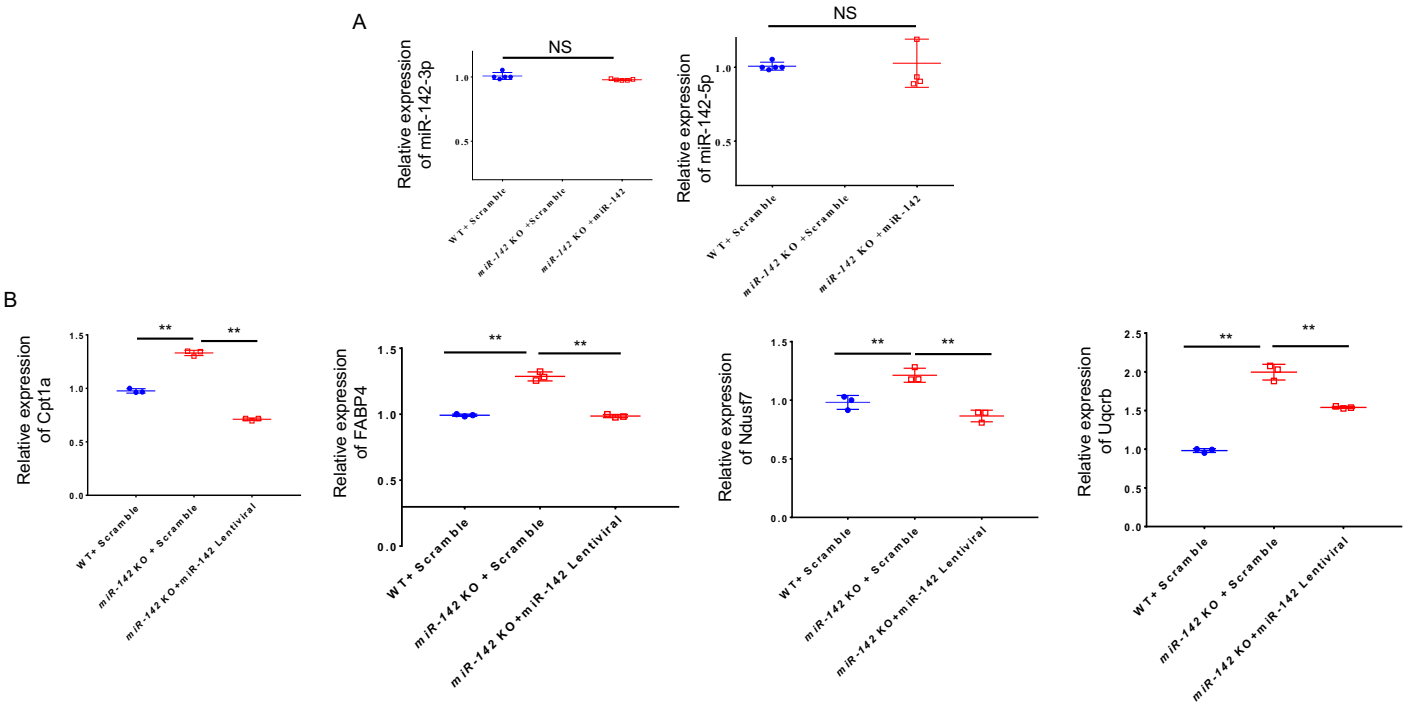

Figure S9: Restoration of miR-142 expression in *miR-142* KO DCs

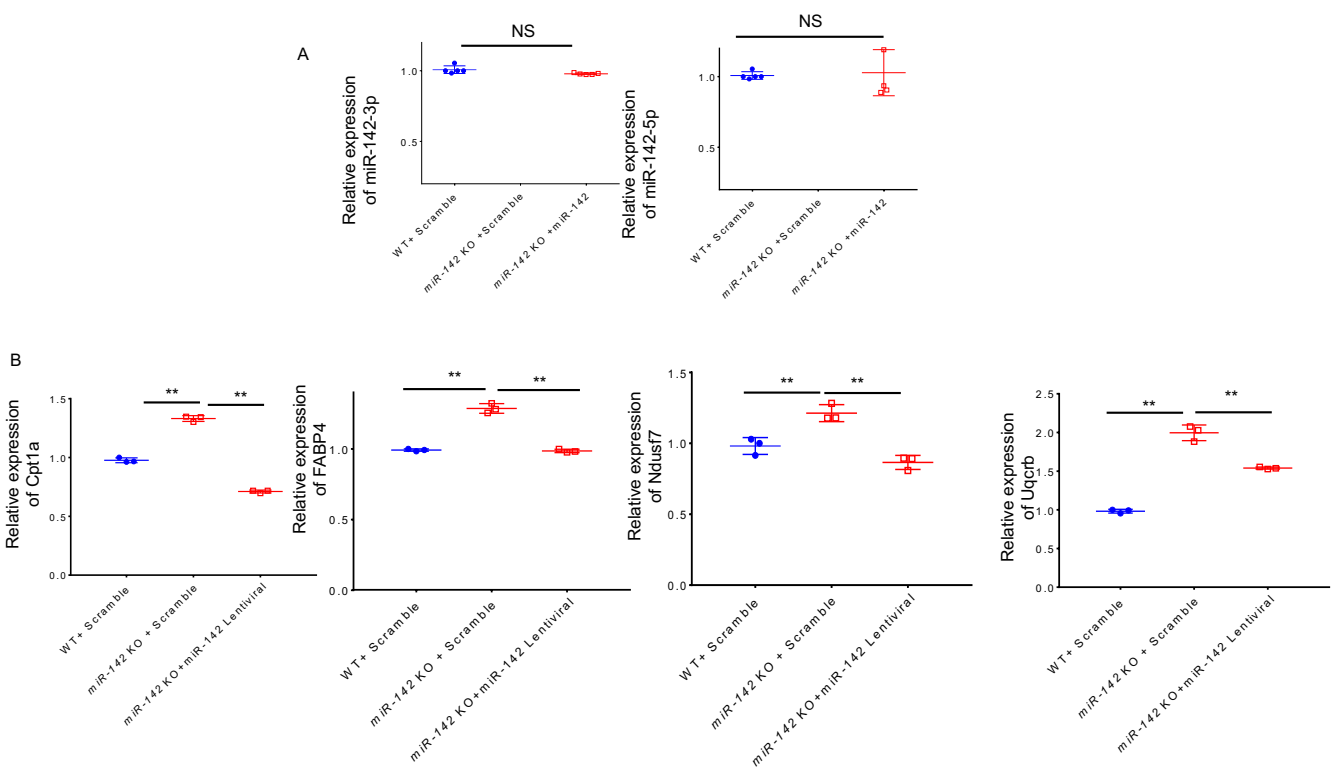

Figure S10: . miR-142 deficiency induced changes in FA Metabolism are critical for modulation of DC functions

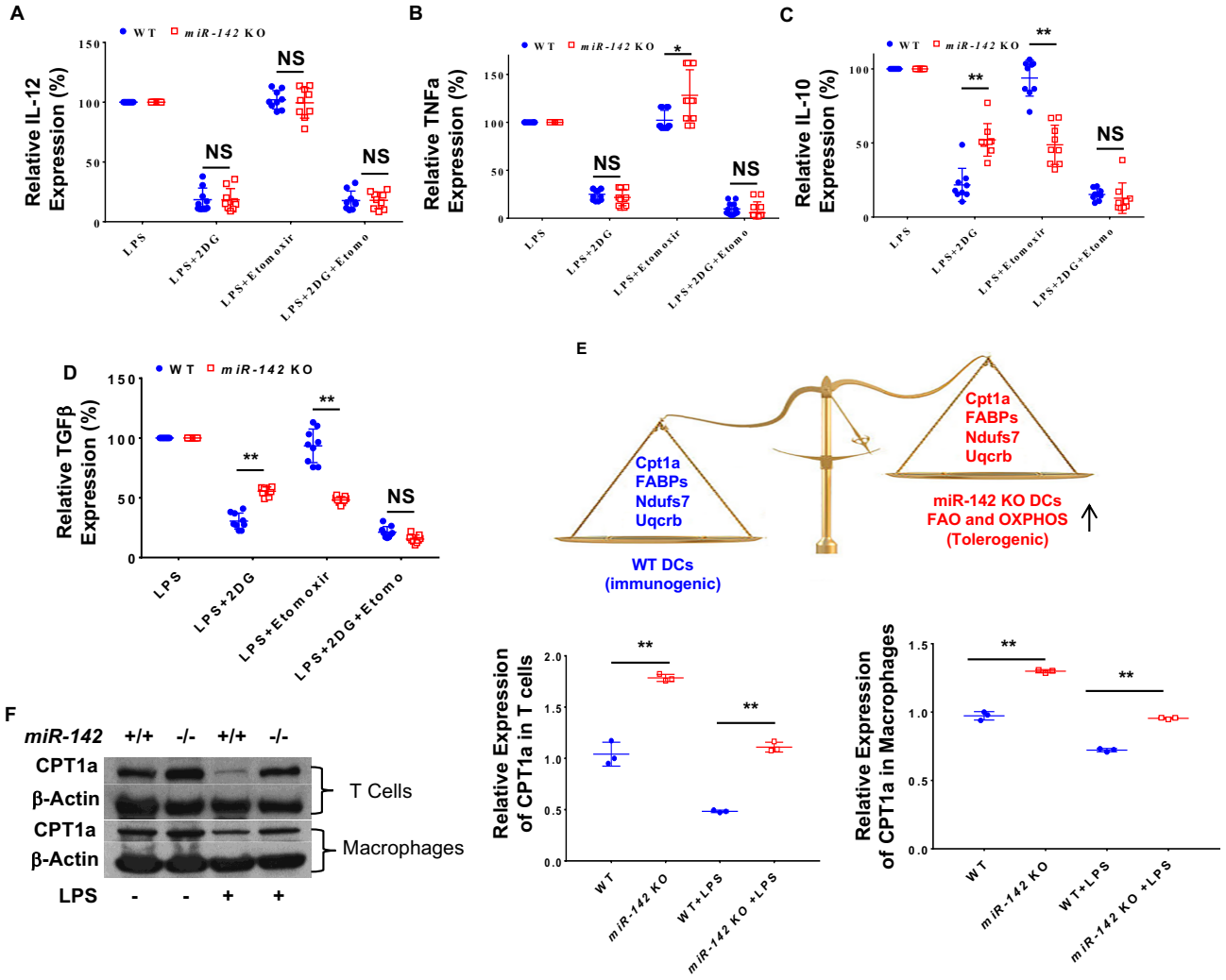

Figure S10: . miR-142 deficiency induced changes in FA Metabolism are critical for modulation of DC functions